
Article:
Al Baroot, A.F. and Grell, M. orcid.org/0000-0003-0714-2039 (2019) Comparing electron- and hole transporting semiconductors in ion sensitive water- gated transistors. Materials Science in Semiconductor Processing, 89. pp. 216-222. ISSN 1369-8001

https://doi.org/10.1016/j.mssp.2018.09.018

Comparing electron- and hole transporting semiconductors in ion sensitive water- gated transistors

Abbad F. Al Baroot[a, b, *]

afalbaroot1@sheffield.ac.uk

Martin Grell[a]

[a]Department of Physics and Astronomy, University of Sheffield, Hicks Building, Hounsfield Road, Sheffield, South ~~Yorkshire, United Kingdom,~~ Yorkshire S3 7RH~~7RH,~~ United Kingdom

[b]Department of Physics, Imam Abdulrahman Bin Faisal University, King Faisal Road, Dammam ~~34212~~34212, Saudi Arabia

[*]Corresponding author ~~at: Department of Physics and Astronomy, University of Sheffield, Hicks Building, Hounsfield Road, Sheffield, South Yorkshire S3 7RH, United Kingdom~~.

Abstract

We present a systematic study comparing different solution-processed semiconductors in cation- sensitive water- gated thin film transistors (WGTFTs): A hole transporting semiconducting polymer (rrP3HT), and an electron- transporting precursor- route metal oxide (ZnO). To allow comparison, we used the same ionophore to sensitise the gate contact for both semiconductors. We find both organic hole transporter and inorganic electron transporter have their relative merits, and drawbacks, in ion- sensitive WGTFTs. Hole transporting rrP3HT WGTFTs show low hysteresis under water- gating and give super- Nernstian sensitivity. However, rrP3HT responds to ionic strength in water even when WGTFTs are not sensitised, compromising selectivity. Electron transporting ZnO WGTFTs show higher mobility, but also stronger hysteresis, and sub- Nernstian response. However, ZnO WGTFTs show little response to ionic strength when not sensitised. We rationalise the super- versus- sub- Nernstian sensitivities via a capacitive amplification/attenuation effect. Our study suggests that the optimum semiconductor material for ion- selective WGTFTs would be a precursor- route inorganic hole transporting semiconductor.

Keywords: ~~water-~~Water- gated thin film transistor; rrP3HT; ~~zinc~~Zinc oxide; ~~crown~~Crown ether; ~~potassium~~Potassium

1 Introduction

The discovery of Kergoat et ~~al~~al. [1] that organic thin film transistors (OTFTs) can be gated using water as an electrolytic gate medium has opened the possibility of using such devices as transducers for the sensing of waterborne analytes. In contrast to the classic ion- sensitive field effect transistor (ISFET [2]), here the sample itself is an active part of the transducer. A number of workers have since demonstrated 'water- gated thin film transistor' (WGTFT) sensors for biologically relevant molecules [3–6], pH [7], and specific cations [8–10], usually by introducing analyte-specific receptors ('sensitisers') into the WGTFT architecture. To sensitise for cations, cation selective 'ionophores' were used, e.g. calixarenes [8–10], or valinomycin [9]. The ionophore was introduced similarly as in conventional electrochemical (potentiometric) cation sensors [e.g. 11,12], namely, by including a plasticised PVC membrane with embedded ionophore in the WGTFT [8,9], or alternatively, dispersed within an organic semiconductor film [10,13]. The threshold of ionophore- sensitised WGTFTs shifted as a result of an ion concentration dependent membrane potential with characteristics logarithmic in ion concentration, similar to Nernstian (more precisely, Nikolsky- Eisenman) characteristics observed in potentiometric ion sensors.

As an alternative to organic semiconductors, solution- processed precursor route inorganic semiconductors have recently gained popularity, as they can be processed with similar ease. Precursors may be metal acetates, chlorides, or nitrates, processed by spin casting and later pyrolysis, or spraying directly onto hot substrates (spray pyrolysis) from solutions in polar solvents or water. Pyrolysis converts such precursors into semiconducting oxides such as ZnO, SnO_2, TiO_2, IGZO or In_2O_3 [14–18]. These metal oxides lead to electron- transporting TFTs, while water- gated organic TFTs usually are hole- transporting. ZnO- based devices in particular have recently been widely used in various sensor devices [19–22].

We present here a systematic study comparing cation- sensitive WGTFTs using either, a hole transporting semiconducting polymer (rrP3HT), or an electron- transporting precursor- route metal oxide (ZnO), as the semiconductor. In both cases, we used a simplified WGTFT architecture, similar as Melzer et ~~al~~al. [9], where the ion- selective membrane was prepared on the gate electrode and analyte solution is used as the gate medium. In the original report on WGTFT ion sensors, List- Kratochvil et ~~al.~~al. [8], had instead used a more complicated two- chamber system where a free-standing membrane separated the analyte from a reference solution, with gating by the reference solution. As ionophore, we used water-insoluble dibenzo crown ether (Dibenzo-30-crown-10, DB30C10, inset Fig. 1) [23,24]. DB30C10 has previously shown sensitivity for potassium [25] and selectivity over sodium (selectivity constant 117) as established by the equipotential method in mixed Na^+/K^+ solutions in a potentiometric ion sensor [26], but so far crown ethers have not been introduced into ion- sensitive WGTFTs.

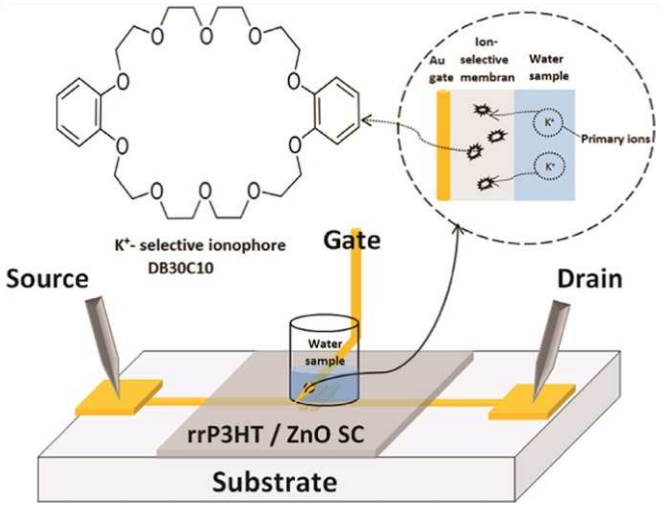

Fig. 1 Design of K^+ sensitive water- gated TFT. Au gate needle sensitised with DB30C10 ionophore embedded in a plasticised PVC membrane. The ionophore's molecular structure is shown in the inset.

alt-text: Fig. 1

2 Experimental

Transistor substrates were prepared by shadow mask evaporation of Au source/drain contact pairs with Cr adhesion layer (contact width W = 1 mm separated by an L = 30 µm channel; W/L = 33.3) onto clean glass substrates. The hole transporting semiconducting polymer regioregular poly(3-hexyl)thiophene (rrP3HT) was purchased from Aldrich (Cat No 698989, electronic grade 99.995% trace metal basis), dissolved at 4 mg/mL in toluene solution, heated gently at 75 °C for ≈ 10 min, and spin cast onto contact substrates at 2000 rpm for 60 s. After casting, films were dried under dynamic vacuum at 120 °C for 1 h. The semicrystalline morphology of rrP3HT films used in sensors has been studied in detail before, e.g. [27–29]. Zinc oxide films were prepared by spraying 3 'puffs' of 100 mM $ZnCl_2$ solution in DI water onto similar TFT substrates heated to 400 °C~~.~~ on a hotplate, which leads to the formation of semiconducting ZnO films('spray pyrolysis', more processing details in [30]). Film thickness was determined with a Veeco Dektak XT surface contact profilometer as 15 nm for rrP3HT and 80 nm for ZnO; ZnO films also are significantly rougher. This agrees with the report of Lehraki *et al.* [31] who showed that spray pyrolysis from zinc chloride precursor leads to highest crystallinity (compared to acetate and nitrate) with largest crystals. This promises higher carrier mobility, but also leads to rougher films and the need for higher thickness to ensure continuity. After spraying, films were first cleaned by DI water, isopropanol, acetone, and UV ozone. Then, ZnO films were treated with hexamethyldisilazane (HMDS) to passivate their amphoteric surface. This was by spraying ~ 1 mL of HMDS into the air inlet of a pre-heated (80 °C)~~.~~ and previously evacuated vacuum oven and keeping films in this atmosphere for 2 h. A goniometer tensiometer coupled with Attension Theta software package was used to determine contact angles of deionized water on rrP3HT and ZnO films.

To prepare K^+ selective membranes, we mixed PVC membrane cocktails from 1.3% of potassium tetrakis [4-chlorophenyl]borate salt, 3.1% 2,3,17,18-Dibenzo-1,4,7,10,13,16,19,22,25,28-decaoxacyclotriaconta-2,17-diene ('DB30C10', Aldrich Cat No 332518) ionophore, 30% poly(vinyl chloride) (PVC), and 65.6% 2-Nitrophenyl octyl ether as plasticiser, similar as in [9]. In total 100 mg of membrane components were dissolved in 3.5 mL of tetrahydrofuran (THF). An L- shaped Au needle was immersed in this solution for several hours, and then dried overnight. In accordance with common practice [e.g. 9, 11], Coated needles were pre-conditioned in 1 mM KCl for several hours. Introducing the ion-sensitive membrane as a coating on the gate needle rather than as a free-standing layer was introduced by Melzer *et al.* [9] for a different ionophore. Aqueous cation solutions were prepared by dissolving KCl or NaCl in deionised (DI) water to a concentration of 100 mM and repeatedly diluted to prepare sample solutions down to 1 nM. Transistors were completed using aqueous cation solutions as electrolytic gate media, starting at the lowest concentration (1 nM) and successively replacing them with solutions of increasing concentration. Electrolyte solutions were held in a small plastic pool of 50 µL capacity that was mounted over the TFT substrate's channel area, as described previously [10]. The solution in the pool was contacted with L- shaped Au needles overlapping the channel along its width to act as a gate contact. Fig. 1 illustrates the resulting WGTFT architecture. To reach equilibrium, we allowed 2 min exposure to electrolyte before each electrical measurement. Then, we recorded transfer characteristics by measuring drain current I_D at drain voltage, $V_D = -0.1$ V for rrP3HT TFTs (+0.1 V for ZnO TFTs), while sweeping gate voltage V_G at 10 mV/s from + 0.2 V to − 0.7 V, and back to + 0.2 V for rrP3HT TFTs (from −0.2 V to +0.7 V and back to −0.2 V for ZnO TFTs). We limited voltage sweeps to 0.7 V rather than the full 'electrochemical window' of water of 1.23 V because it was shown previously that rrP3HT long-term stability may be compromised at higher voltages [8]. Results are presented on a linear drain current (I_D) scale, and 'master curves' were constructed by shifting transfer characteristics along the gate voltage axis until they best matched with the 1 nM characteristic. Carrier mobility was evaluated from master curves with standard transistor equations, assuming a capacitance of 3 µF/cm^2 [1]. The

required shift along the gate voltage axis was taken as the threshold shift under respective ion concentration and was fitted to the Nikolsky- Eisenman equation (Eq. (2) below) with the nonlinear fit routine in Origin software.

3 Results and discussion

Fig. 2a shows families of rrP3HT WGTFT linear transfer characteristics when contacted with a gate needle coated in DB30C10- sensitised PVC membrane, and gated with aqueous potassium solutions in the concentration range ~~1~~(1 nM ... ~~100~~100 mM). The transfer characteristic under deionised ('MilliQ') water (c = 0) is not shown here as it is effectively indistinguishable from the characteristics under ~~1~~1 nM K^+, and later data analysis is on a logarithmic concentration scale which does not allow to show data for c ~~= 0.~~ = 0. All transfer characteristics are typical of the hole- transporting TFTs: Once the gate voltage is more negative than a threshold, the TFT delivers a negative drain current of increasing magnitude as the gate voltage is made increasingly negative. Also, Fig. 2a clearly shows that threshold becomes more negative, i.e. shifts away from zero, with increasing concentration c ~~= [K~~= $[K^+]$ for c above ~~100~~100 nM, suggesting a limit- of- detection for potassium in the range ~~(100~~(100 nM ... ~~1~~1 µM). We find that all recorded transfer characteristics for $[K^+]$ ~~> 1~~> 1 nM can be brought to overlap with the $[K^+]$ ~~= 1~~= 1 nM characteristic by shifting them along the gate voltage axis by a concentration-dependent voltage shift, $\Delta V_T(c)$. As WGTFTs often display some hysteresis in the transfer characteristics, we here matched at the 'rising' flank of the hysteresis loop, i.e. when sweeping gate voltage from 'off' (near- zero gate voltage) to 'on', namely to increasingly negative gate voltage for a hole transporting semiconductor. However, hysteresis is small for rrP3HT WGTFTs. The resulting 'master curve' is shown in Fig. 2b. In this way, we determine a threshold shift without assuming a specific model of the $I_D(V_G)$ characteristic. In Fig. 2b and all future master curves, the gate voltage axis therefore does not show the actually applied gate voltage, but an 'effective' gate voltage that is corrected for the threshold shift,(effective V_G = applied V_G - $\Delta V_T(c)$). The required shift $\Delta V_T(c)$ is shown and analysed in context with other data in Fig. 10 and Table 1 ~~below~~. Note that Giridharagopal et al. [32] have reported increased drain currents for non- sensitised rrP3HT WGTFTs under high concentrations ~~(10 to 100~~(10–100 mM) of KCl, which they assigned to some penetration of chloride anions into the rrP3HT film. We can clearly exclude this here, as currents in Fig. 2a are lower, not higher, under high KCl concentrations.

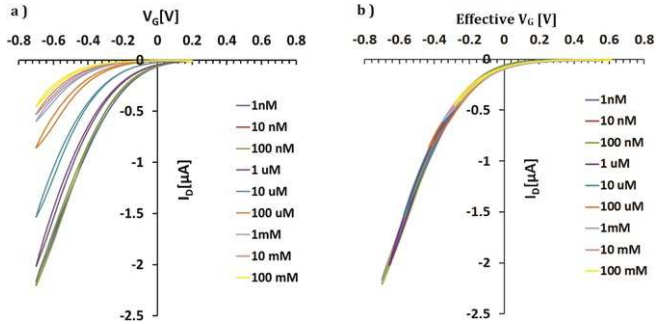

Fig. 2 a: Transfer Characteristics of water- gated rrP3HT TFTs contacted by an Au gate needle sensitised with DB30C10 ionophore embedded in a plasticised PVC membrane. Gating is with water with different concentrations of potassium (K^+, from KCl), increasing from ~~1~~1 nM ... ~~100~~100 mM in factors of 10. **b:** Transfer characteristic 'master curve' constructed by shifting characteristics along the gate voltage axis to give the best possible overlap with the characteristic under lowest ~~(1~~(1 nM) K^+ concentration.

alt-text: Fig. 2

Table 1 contact angles, carrier mobilities, and the fit parameters to $\Delta V_T(c)$ according to Eq. (2), for the different WGTFTs studied here. Fit parameters evaluated by the Origin nonlinear fit routine.

alt-text: Table 1

Semiconductor	Contact angle [°]~~o~~	Ion	µ [cm^2/Vs]	c_{st} [nM]	s [mV/dec]
rrP3HT	102	K^+	0.45 (h^+)	160 ± 72	77 ± 3
rrP3HT	102	Na^+	0.45 (h^+)	9060 ± 9090	47 ± 7
HMDS-ZnO	86.5	K^+	15(e^-)	65 ± 57	36 ± 4
HMDS-ZnO	86.5	Na^+	6.25(e^-)	313 ±131	19 ± 1

The ability to construct master curves by shifting transfer characteristics along gate voltage axis (here and also later in Figs. 2b–9b) does establish that $\Delta V_T(c)$ reflects only a shift of gate membrane potential in response to K^+ concentration, without concentration-dependent changes of carrier mobility or electrolyte capacitance. Otherwise, the transfer characteristics above threshold would differ in their slopes and would not project onto a single master

curve, ~~cf.~~cf. Eq. (1) below. On the level of transistor operation that means K^+ ions in the gate medium do not interfere with carrier transport in the semiconductor, and the dependency of electrolyte capacitance on ion concentration is weak. The latter is reasonable as there will always be sufficient ions to populate a very thin double layer, which can migrate there from the droplet bulk.

Figs. 3–5 show three control experiments on rrP3HT WGTFTs. The response of DB30C10- sensitised rrP3HT WGTFTs to sodium instead of potassium in the gating water is shown in Fig. 3, probing the selectivity of the sensor against an 'interferant'. Figs. 4 and 5 show the response of rrP3HT WGTFT to K^+ and Na^+ respectively, when the gate contact was not sensitised. Corresponding $\Delta V_T(c)$ are also shown and analysed in context in Fig. 11 and Table 1 ~~below~~

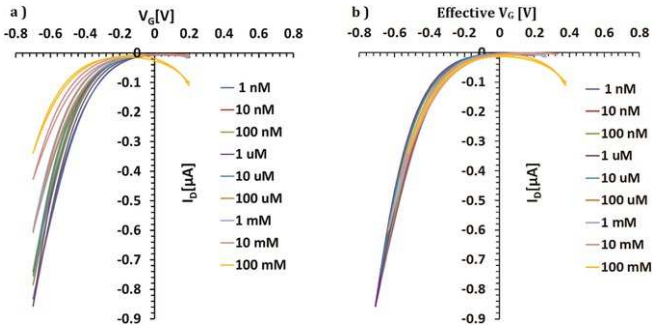

Fig. 3 a Transfer Characteristics of water- gated rrP3HT TFTs contacted by an Au gate needle sensitised with DB30C10 ionophore embedded in a plasticised PVC membrane. Gating is with water with different concentrations of sodium (Na^+, from NaCl), i.e. an interferant, increasing from ~~1~~1 nM ... ~~100~~100 mM in factors of 10. **b:** Transfer characteristic 'master curve' constructed by shifting characteristics along the gate voltage axis to give the best possible overlap with the characteristic under lowest ~~(~~(1 nM) Na^+ concentration.

alt-text: Fig. 3

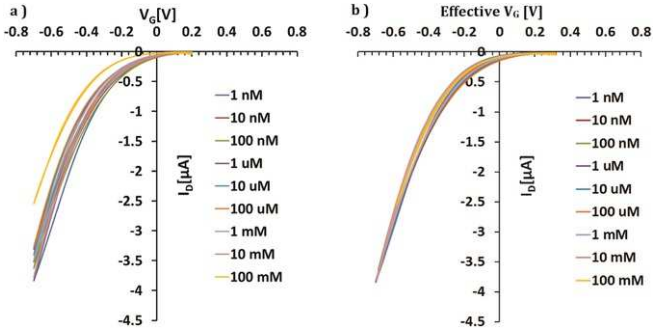

Fig. 4 a: Transfer Characteristics of water- gated rrP3HT TFTs contacted by an unsensitised Au gate needle as a control experiment. Gating is with water with different concentrations of potassium (K^+, from KCl), increasing from ~~1~~1 nM ... ~~100~~100 mM in factors of 10. **b:** Transfer characteristic 'master curve' constructed by shifting characteristics along the gate voltage axis to give best possible overlap with the characteristic under lowest ~~(~~(1 nM) K^+ concentration.

alt-text: Fig. 4

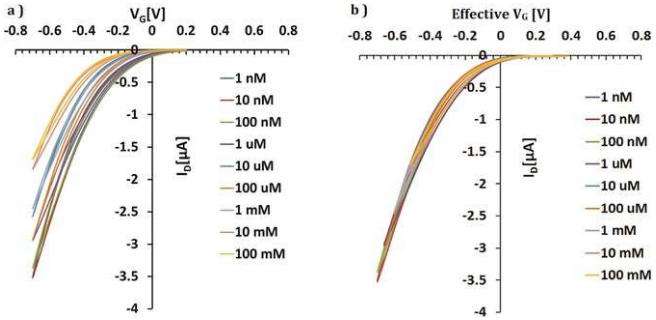

Fig. 5 a: Transfer Characteristics of water- gated rrP3HT TFTs contacted by an unsensitised Au gate needle as a control experiment. Gating is with water with different concentrations of sodium (Na^+, from NaCl), increasing from ~~1~~1 nM ... ~~100~~100 mM in factors of 10. **b:** Transfer characteristic 'master curve' constructed by shifting characteristics along the gate voltage axis to give best possible overlap with the characteristic under lowest ~~(1~~(1 nM) Na^+ concentration.

alt-text: Fig. 5

Figs. 6–9 show the corresponding set of experiments using spray pyrolysed and HMDS- treated ZnO rather than rrP3HT as semiconductor: Fig. 6, sensitised ZnO transistor under K^+, Fig. 7: sensitised ZnO WGTFT under Na^+ 'interferant', Figs. 8 and 9 non- sensitised ZnO WGTFT.

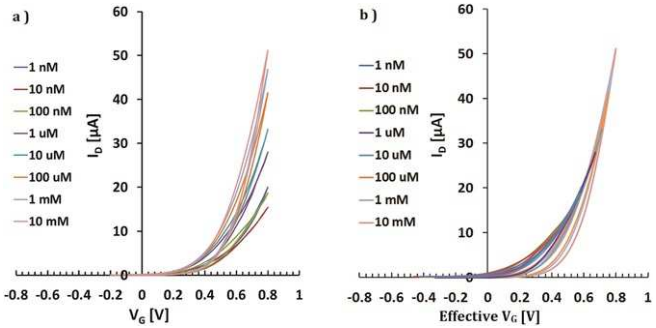

Fig. 6 a: Transfer Characteristics of water- gated HMDS- treated ZnO TFTs contacted by an Au gate needle sensitised with DB30C10 ionophore embedded in a plasticised PVC membrane. Gating is with water with different concentrations of potassium (K^+, from KCl), increasing from ~~1~~1 nM ... ~~10~~10 mM in factors of 10. **b:** Same transfer characteristics as in 2a but shifted along the gate voltage axis for best overlap with the $[K^+]$ ~~= 1~~= 1 nM characteristic. Characteristics were matched at the 'rising' flank, i.e. when sweeping gate voltage from near zero to large positive values.

alt-text: Fig. 6

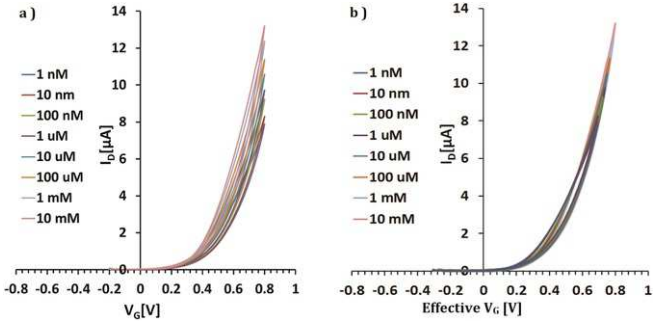

Fig. 7 a: Transfer Characteristics of water- gated HMDS- treated ZnO TFTs contacted by an Au gate needle sensitised with DB30C10 ionophore embedded in a plasticised PVC membrane. Gating is with water with different concentrations of sodium (Na^+, from NaCl) i.e. an interferant, increasing from ~~1~~1 nM ... ~~10~~10 mM in factors of 10. **b:** Same transfer characteristics as in 6a but shifted along the gate voltage axis for best overlap with the $[Na^+]$ ~~= 1~~= 1 nM characteristic. Characteristics were matched at the

'rising' flank, i.e. when sweeping gate voltage from zero to positive values.

alt-text: Fig. 7

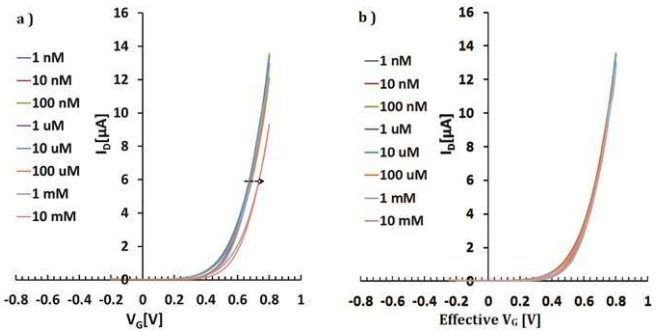

Fig. 8 a: Transfer Characteristics of water- gated HMDS-treated ZnO TFTs contacted by an unsensitised Au gate needle as a control experiment. Gating is with water with different concentrations of potassium (K^+, from KCl), increasing from ~~1~~1 nM ... ~~10~~10 mM in factors of 10. **b:** Transfer characteristic 'master curve' constructed by shifting characteristics along the gate voltage axis to give best possible overlap with the characteristic under lowest ~~1~~(1 nM) K^+ concentration.

alt-text: Fig. 8

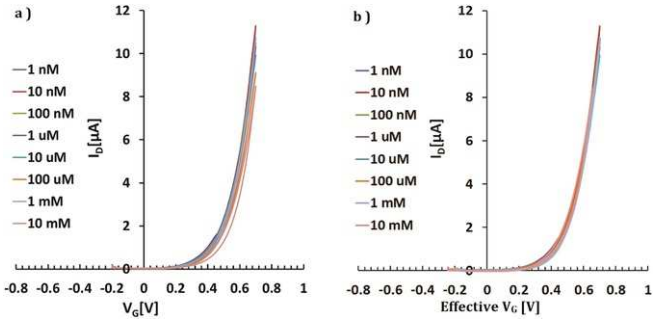

Fig. 9 a: Transfer Characteristics of water- gated HMDS-treated ZnO TFTs contacted by an unsensitised Au gate needle as a control experiment. Gating is with water with different concentrations of sodium (Na^+, from NaCl), increasing from ~~1~~1 nM ... ~~10~~10 mM in factors of 10. **b:** Transfer characteristic 'master curve' constructed by shifting characteristics along the gate voltage axis to give best possible overlap with the characteristic under lowest ~~1~~(1 nM) Na^+ concentration.

alt-text: Fig. 9

Now transfer characteristics are typical of electron- transporting TFTs: Once the gate voltage is more positive than a threshold, the TFT delivers a positive drain current of increasing magnitude as the gate voltage is made increasingly positive. Fig. 6a shows threshold shifts in the same direction as for rrP3HT TFTs. However, this now means threshold becomes less positive with increasing K^+ concentration, shifting towards zero from an initially larger positive threshold rather than away from zero from an initially smaller negative value for rrP3HT WGTFTs. Also, the shift is now smaller in magnitude, and hysteresis is significant in particular for high ion concentration. We again constructed a 'master curve' (Fig. 6b) by shifting along the gate voltage axis. Characteristics were again matched at the 'rising' flank, which now is observed when sweeping gate voltage from near zero to large positive voltage as ZnO is an electron transporter. On the rising flanks, the different transfer characteristics again overlap well into a single master curve, the apparent mismatch of some characteristics is due to hysteresis on the 'falling' flank, sweeping gate voltage back towards zero. The required shift $\Delta V_T(c)$ is shown and analysed in context in Fig. 11 and Table 1 below. Figs. 7-9 show three control experiments on ZnO WGTFTs. The response of DB30C10- sensitised ZnO WGTFTs to sodium instead of potassium in the gating water is shown in Fig. 7. Figs. 8 and 9 show the response of ZnO WGTFT to K^+ and Na^+ respectively when the gate contact was not sensitised. Corresponding $\Delta V_T(c)$ are also shown and analysed in context in Fig. 11 and Table 1 ~~below~~.

Charge carrier mobility in the studied WGTFTs can be extracted from the linear transfer characteristic 'master curves', Figs., 2b, 3b, 6b and 7b. Simple TFT theory relates charge carrier mobility, µ, to the (linear) transconductance (g_m)via Eq. (1):

$$g_m = W/L\ \mu C_i V_D \quad \textbf{(1)}$$

Wherein linear transconductance is defined as the slope of the linear transfer characteristic ($|V_D| \ll |V_G - V_T|$), g_m ~~= ∂I~~= $\partial I_D/\partial V_G$. C_i is the capacitance of the gate medium and ~~W/L = 33.3~~ W/L = 33.3 for our TFT substrates. We fitted straight lines in the high gate voltage regimes (V_G > ~~500~~500 mV) of our master curves to find g_m and esti$_m$ate the specific capacitance of the aqueous gate medium as 3 µF/cm^2 [1]. Eq. (1) then allows calculation of carrier mobilities, results are summarised in Table 1. We find higher mobilities in ZnO than in rrP3HT; our results overlap with previous reports of mobilities in water- gated rrP3HT [10,33] and precursor- route ZnO TFTs [14,30,34].

Threshold shift $\Delta V_T(c)$ in ion- sensitive WGTFTs is rationalised as the result of an ion concentration-dependent membrane potential, $V_M(c)$ [8,9], which is effectively added to the gate contact's work function, and hence to TFT threshold voltage. For quantitative analysis, the $\Delta V_T(c)$ required to construct the master curves in Figs. 2b–9b are plotted vs. a logarithmic concentration scale in Figs. 10 and 11 respectively. Also included are $\Delta V_T(c)$ for non- sensitised WGTFTs. For quantitative analysis, we fitted $\Delta V_T(c)$ according to the Nikolsky- Eisenman equation that describes ion concentration dependency of membrane potentials [35],

$$-\Delta V_T(c) = V_0 + s \log(c + c_{st}) \quad -\Delta V_T(c) = V_0 + s \log(c + c_{st}) \qquad \textbf{(2)}$$

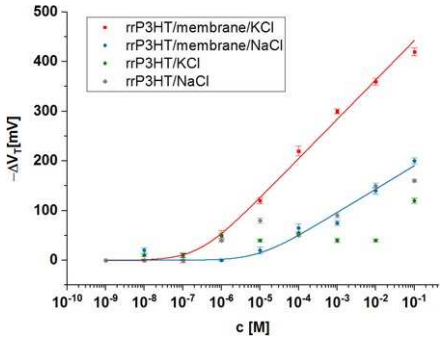

Fig. 10 Threshold shifts $\Delta V_T(c)$ under increasing concentration c of potassium or sodium in the gating water for rrP3HT WGTFTs sensitised with DB30C10/PVC membranes: red squares, potassium (from KCl); blue circles: Sodium (from NaCl). Solid lines are fits to Eq. (2); fit parameters are summarised in Table 1. Also shown, response without ion- sensitive membrane: green circle, potassium (from KCl); grey squares: Sodium (from NaCl).

alt-text: Fig. 10

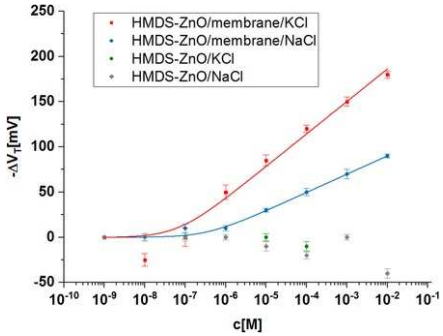

Fig. 11 Threshold shifts $\Delta V_T(c)$ under increasing concentration c of potassium or sodium in the gating water for ZnO WGTFTs sensitised with DB30C10/PVC membranes: red squares, potassium (from KCl); blue circles: Sodium (from NaCl). Solid lines are fits to Eq. (2); fit parameters are summarised in Table 1. Also shown, response without ion- sensitive membrane: green circles, potassium (from KCl); grey squares: Sodium (from NaCl).

alt-text: Fig. 11

We here neglect the distinction between concentration and activity. V_0 ~~= -s~~ = -s log ~~(1~~(1 nM + c_{st}) ensures ΔV_T ~~(1~~(1 nM)~~nM) = 0~~ = 0 as implied by the shift procedure. Eq. (2) has two free fit parameters, s and c_{st}. For c >> c_{st}, Eq. (2) agrees with the generic Nernst equation (e.g. [8]). s is a slope (in mV / decade) that quantifies sensitivity; according to Nernst ~~s = 58/z~~ s = 58/z mV/dec (at ambient temperature, wherein z is the ion's valency, ~~z = 1~~ z = 1 for K^+ and Na^+ [e.g. [8]~~)~~]. c_{st} sets a limit of detection (LoD), c_{st} ~~≈ LoD.~~ ≈ LoD. The s and c_{st} we find from fitting data in Figs. 10 and 11 are summarised in Table 1, together with contact angles and carrier mobilities.

According to Nikolsky-Eisenman theory, the selectivity of an ionophore for an analyte- over an interferant ion is quantified by the ratio of their c_{st}, while slope s above c_{st} should match the Nernstian value ~~s = 58/z~~ s = 58/z mV/dec. However, it is known from many experimental studies, including WGTFTs and potentiometric transducers, that slope s under interferant often is lower than for analyte ion even above c_{st} [e.g. 8,9,11].

As we always used the same DB30C10- sensitised PVC membrane on the WGTFT's gate contact, membrane potential $V_M(c)$ is expected to be the same for all WGTFTs tested here. Yet remarkably, we find the observed $\Delta V_T(c)$ are not equal: Hole- transporting rrP3HT WGTFTs display a 'super- Nernstian' potassium sensitivity of $s = 77 \pm 3$ mV/dec, while we find only $s = 36 \pm 4$ mV/dec for electron- transporting ZnO TFTs. We note that a WGTFT is gated across a series of two electric double layer (EDL) capacitors: For a hole transporting WGTFT, a cationic EDL forms at the gate electrode/water interface in series with an anionic EDL at the water/semiconductor interface. For an electron transporting WGTFT, EDL sequence is reversed. Apparently, the EDL sequence for gating ZnO leads to larger hysteresis (compare Figs. 2b–6b), which in itself warrants further investigation, but as threshold shift was evaluated from matching at the 'rising' flanks only, hysteresis cannot account for super- ~~vs.~~vs. sub- Nernstian sensitivity. However, we expect the cationic EDL to display higher capacitance than the anionic EDL due to the smaller size of cations. As both EDLs carry the same charge, the lower capacitance (anionic) EDL must therefore display a higher potential difference across it. As it is the anionic EDL that gates the hole- transporting semiconductor, we believe this leads to a sensitivity amplification for hole transporting WGTFTs according to the EDL capacitance ratio. A similar capacitive amplification was achieved by Spijkman et ~~al.~~al. [36] in a dual- gate architecture, albeit not in a water- gated TFT. For an electron transporting WGTFT, EDL sequence is reversed, leading to sub- Nernstian response in our ZnO WGTFTs. Previous reports are consistent with the above, albeit they have not been explained in those terms by their authors: Melzer et *al.* [9] report sub- Nernstian $s = 39.3 \pm 1.6$ mV/dec for sensing potassium using electron transporting carbon nanotubes, while Althagafi ~~et al.~~et al. [12] found super- Nernstian response (55 mV/dec for Ca^{2+}, here $z = 2$ hence Nernstian slope would be only 29 mV/dec) using hole transporting polymer poly(2,5-bis(3-hexadecylthiophen-2-yl)thieno[3,2-b]thiophene) (PBTTT). Note that in the original report on an ion- sensitive WGTFT by List- Kratochvil et ~~al.~~al. [8], the authors used a two-chamber system separated by the ion-sensitive membrane, rather than preparing it on the gate electrode. This leads to a serial combination of 4 (not 2) EDLs in alternating order, cancelling amplification.

Both DB30C10- sensitised rrP3HT and ZnO WGTFTs also respond to the'interferant' Na^+ albeit with higher LoD, and almost halved s even above LoD, compared to the primary analyte, K^+. This reflects the (limited) selectivity of the DB30C10 ionophore [26] but is not a feature of the chosen device architecture or semiconductor.

While the above discussion suggests rrP3HT as the preferred semiconductor for ion sensing with WGTFTs (lower hysteresis, super- Nernstian response), Fig. 10 reveals that unfortunately, even unsensitised rrP3HT WGTFTs display some response to increasing K^+ and Na^+ concentration, simply due to increasing ionic strength of the gating solution. It is known that organic semiconductor films have some permeability to ions [37,38] which we believe leads to the observed threshold shift under increasing ion concentration, even in the absence of a selective membrane particularly for the smaller Na^+ ions. Unspecific threshold shift due to increasing ionic strength can be avoided by using two- chamber architecture as by List-Kratochvil et ~~al.~~al. [8], but at the expense of more complicated device architecture, and the loss of capacitive sensitivity enhancement.

Alternatively, we can use ZnO as a semiconductor, which apparently is impermeable to ions. Fig. 11 shows that for unsensitised ZnO WGTFTs, increasing ionic strength only leads to small threshold shift at very high ion concentrations, and with an opposite sign as for sensitised WGTFTs, which allows for clear distinction from membrane- induced threshold shift. While ZnO has the added (minor) advantage of higher carrier mobility, hence higher TFT currents, this comes at the expense of higher hysteresis, and a reversal of the favourable capacitive sensitivity enhancement found for p-type semiconductors.

4 Summary and conclusions

We compare ion- sensitive water- gated (WG) electric double layer (EDL) thin film transistors (TFTs) using p-type (organic) vs. n-type (inorganic) solution-processed semiconductors. Both types of WGTFTs were sensitised at the gate contact with PVC membranes containing the potassium- selective ionophore DB30C10. DB30C10 has been investigated previously in conventional potentiometric ion sensors [26], but not yet in WGTFTs. When using the organic polymer hole transporter rrP3HT as semiconductor, we observe TFT transfer characteristics with little hysteresis, and super- Nernstian potassium sensitivity of ~~77 +/- 3~~77 ± 3 mV/decade. We explain super- Nernstian response as capacitive amplification by the ratio of cationic/anionic EDL capacitance. However, control experiments reveal a weaker, non- selective ion response of rrP3HT itself, in the absence of an ion- sensitive membrane. This compromises ion selectivity. To retain selectivity, a two- chamber design would be required that avoids direct contact between semiconductor and analyte solution [8]. However, this adds significant complexity to device manufacture and loses super-Nernstian response.

By contrast, WGTFTs using the electron- transporting inorganic II-VI semiconductor Zinc oxide (ZnO) sprayed from soluble precursor display higher mobility, stronger hysteresis, and sub- Nernstian response when sensitised with DB30C10 membranes. Sub- Nernstian response has been observed previously for n-type ion selective WGTFTs [9], we explain this by the now reversed sequence of cationic/anionic EDLs. However, other than rrP3HT, unsensitised ZnO WGTFTs are less responsive to ionic strength in the gating water. This retains the membrane's ion selectivity without the need for a two-chamber device design.

Hence, both organic p-type, and inorganic n-type solution-processed semiconductors have their relative merits, and drawbacks, for use in ion-selective WGTFTs. Our study suggests that the optimum semiconductor material for ion- selective WGTFTs would be an impermeable precursor- route inorganic p-type semiconductor, combining favourable capacitive sensitivity amplification, and indifference to ionic strength. To our knowledge, no such material is yet available.

Acknowledgments

Abbad Al Baroot thanks the Cultural Attaché of Saudi Arabia to the UK and Imam Abdulrahman Bin Faisal University~~Imam Abdulrahman Bin Faisal University, ~~Saudi Arabia, for providing him with a fellowship for his

Ph.D. studies.

References

[1] L. Kergoat, et al., A water-gate organic field-effect transistor, ~~*Advanced materials*~~*Adv. Mater.* ~~22~~**22** (23), 2010, 2565–2569.

[2] P. Bergveld, Thirty years of ISFETOLOGY: What happened in the past 30 years and what may happen in the next 30 years, ~~*Sensors and*~~ *Sens. Actuators B:* ~~*Chemica*~~*Chem.* ~~88~~**88** (1), 2003, 1–20.

[3] F. Buth, et al., Biofunctional electrolyte-gated organic field-effect transistors, ~~*Advanced materials*~~*Adv. Mater.* ~~24~~**24** (33), 2012, 4511–4517.

[4] S. Casalini, et al., Organic field-effect transistor for label-free dopamine sensing, ~~*Organic Electronics*~~*Org. Electron.* ~~14~~**14** (1), 2013, 156–163.

[5] S.A. Algarni, et al., A water-gated organic thin film transistor as a sensor for water-borne amines, *Talanta* ~~153~~**153**, 2016, 107–110.

[6] R.F. de Oliveira, et al., Water-gated phthalocyanine transistors: ~~Operation~~operation and transduction of the peptide–enzyme interaction, ~~*Organic Electronics*~~*Org. Electron.* ~~31~~**31**, 2016, 217–226.

[7] S. Panda, Enhanced pH sensitivity over the Nernst limit of electrolyte gated a-IGZO thin film transistor using branched polyethylenimine, *RSC* ~~*advances*~~*Adv.* ~~6~~**6**, 2016, 10810–10815.

[8] K. Schmoltner, et al., Electrolyte-gated organic field-effect transistor for selective reversible ion detection, ~~*Advanced materials*~~*Adv. Mater.* ~~25~~**25** (47), 2013, 6895–6899.

[9] K. Melzer, et al., Selective ion-sensing with membrane-functionalized electrolyte-gated carbon nanotube field-effect transistors, *Analyst* ~~139~~**139** (19), 2014, 4947–4954.

[10] T.M. Althagafi, et al., A membrane-free cation selective water-gated transistor, *Analyst* ~~141~~**141** (19), 2016, 5571–5576.

[11] S.K. Menon, et al., Azo calix[4]arene based neodymium(III)-selective PVC membrane sensor, *Talanta* ~~83~~**83** (5), 2011, 1329–1334.

[12] A. Michalska, K. Pyrzyńska and K. Maksymiuk, Method of achieving desired potentiometric responses of polyacrylate-based ion-selective membranes, ~~*Analytical chemistry*~~*Anal. Chem.* ~~80~~**80** (10), 2008, 3921–3924.

[13] T.M. Althagafi, S.A. Algarni and M. Grell, Innate cation sensitivity in a semiconducting polymer, *Talanta* ~~158~~**158**, 2016, 70–76.

[14] B.S. Ong, et al., Stable, solution-processed, high-mobility ZnO thin-film transistors, ~~*Journal of the American Chemical Society*~~*J. Am. Chem. Soc.* ~~129~~**129** (10), 2007, 2750–2751.

[15] G. Adamopoulos, et al., ~~High-Mobility Low-Voltage~~high-mobility low-voltage ZnO and ~~Li-Doped~~Li-doped ZnO ~~Transistors Based~~transistors based on ZrO2 ~~High-k Dielectric Grown~~high-k dielectric grown by ~~Spray Pyrolysis~~spray pyrolysis in ~~Ambient Air~~ambient air, ~~*Advanced materials*~~*Adv. Mater.* ~~23~~**23** (16), 2011, 1894–1898.

[16] Y.-H. Yang, et al., Chemical and ~~Electrical Properties~~electrical properties of ~~Low-Temperature Solution-Processed~~low-temperature solution-processed In–Ga–Zn-O ~~Thin-Film Transistors~~thin-film transistors, *IEEE Electron Device* ~~*Letters*~~*Lett.* ~~31~~**31** (4), 2010, 329–331.

[17] J.-Y. Bae, et al., Facile ~~Route~~route to the ~~Controlled Synthesis~~controlled synthesis of ~~Tetragonal~~tetragonal and ~~Orthorhombic~~orthorhombic SnO2 ~~Films~~films by ~~Mist Chemical Vapor Deposition~~mist chemical vapor deposition, *ACS* ~~*applied materials & interfaces*~~*Appl. Mater. Interfaces* ~~7~~**7** (22), 2015, 12074–12079.

[18] I. Isakov, et al., Exploring the ~~Leidenfrost Effect~~leidenfrost effect for the ~~Deposition~~deposition of ~~High-Quality~~high-quality In2 O3 ~~Layers~~layers via ~~Spray Pyrolysis~~spray pyrolysis at ~~Low Temperatures~~low temperatures and ~~Their Application~~their application in ~~High Electron Mobility Transistors~~high electron mobility transistors, ~~*Advanced Functional Materials*~~*Adv. Funct. Mater.* 2017, 1606407.

[19] R. Ahmad, M.-S. Ahn and Y.-B. Hahn, Fabrication of a non-enzymatic glucose sensor field-effect transistor based on vertically-oriented ZnO nanorods modified with Fe2O3, ~~*Electrochemistry Communications*~~*Electrochem. Commun.* ~~77~~**77**, 2017, 107–111.

[20] R. Ahmad, M.-S. Ahn and Y.-B. Hahn, ZnO nanorods array based field-effect transistor biosensor for phosphate detection, ~~*Journal of colloid and interface science*~~*J. Colloid Interface Sci.* ~~498~~**498**, 2017, 292–297.

[21] R. Ahmad and Y.-B. Hahn, Nonenzymatic flexible field-effect transistor based glucose sensor fabricated using NiO quantum dots modified ZnO nanorods, ~~*Journal of colloid and interface science*~~*J. Colloid Interface Sci.* ~~512~~**512**, 2018, 21–28.

[22] R. Ahmad, et al., Recent advances in nanowires-based field-effect transistors for biological sensor applications, ~~*Biosensors and Bioelectronics*~~*Biosens. Bioelectron.* 2017.

[23] C.J. Pedersen, Cyclic polyethers and their complexes with metal salts, ~~*Journal of the American Chemical Society*~~*J. Am. Chem. Soc.* ~~**89**~~**89** (26), 1967, 7017–7036.

[24] C.J. Pedersen, Macrocyclic ~~Polyethers. Dibenzo-18-Crown-6 Polyether~~polyethers: dibenzo-18-crown-6 polyether and ~~Dicyclohexyl-18-Crown-6 Polyether~~dicyclohexyl-18-crown-6 polyether, ~~*Organic Syntheses*~~*Org. Synth.* ~~**52**~~**52**, 1972, 66.

[25] D. Lee and J. Thomas, ~~4~~4′-picrylamino-5′-nitrobenzo-18-crown-6~~-picrylamino-5~~ as~~-nitrobenzo-18-crown-6 as a sensing reagent in potassium ion-selective electrode membranes~~ a sensing reagent in potassium ion-selective electrode membranes, *Talanta* ~~**41**~~**41** (6), 1994, 901–907.

[26] J. Petranek and O. Ryba, Potassium-selective electrodes based on macrocyclic polyethers: ~~The~~the effect of structure of the neutral carrier on selectivity, ~~*Analytica Chimica*~~*Anal. Chim. Acta* ~~**72**~~**72** (2), 1974, 375–380.

[27] J.Y. Na, et al., Understanding solidification of polythiophene thin films during spin-coating: effects of spin-coating time and processing additives, ~~*Scientific reports*~~*Sci. Rep.* ~~**5**~~**5**, 2015, 13288.

[28] J.W. Jeong, et al., The response characteristics of a gas sensor based on poly-3-hexylithiophene thin-film transistors, ~~*Sensors and* ~~*Sens. Actuators B:* ~~*Chemical*~~*Chem.* ~~**146**~~**146** (1), 2010, 40–45.

[29] K. Manoli, et al., A comparative study of the gas sensing behavior in P3HT-and PBTTT-based OTFTs: ~~The~~the influence of film morphology and contact electrode position, *Sensors* ~~**14**~~**14** (9), 2014, 16869–16880.

[30] T.M. Althagafi, A.F. Al Baroot and M. Grell, A new precursor route to semiconducting ~~Zinc Oxide~~zinc oxide, *IEEE Electron Device* ~~*Letters*~~*Lett.* ~~**37**~~**37** (10), 2016, 1299–1302.

[31] N. Lehraki, et al., ZnO thin films deposition by spray pyrolysis: ~~Influence~~influence of precursor solution properties, ~~*Current Applied Physics*~~*Curr. Appl. Phys.* ~~**12**~~**12** (5), 2012, 1283–1287.

[32] R. Giridharagopal, et al., Electrochemical strain microscopy probes morphology-induced variations in ion uptake and performance in organic electrochemical transistors, ~~*Nature materials*~~*Nat. Mater.* ~~**16**~~**16** (7), 2017, 737.

[33] A. Nawaz, et al., High mobility organic field-effect transistors based on defect-free regioregular poly (3-hexylthiophene-2, 5-diyl), ~~*Organic Electronics*~~*Org. Electron.* ~~**38**~~**38**, 2016, 89–96.

[34] T.M. Althagafi, et al., Precursor-route ZnO films from a mixed casting solvent for high performance aqueous electrolyte-gated transistors, ~~*Physical Chemistry Chemical Physics*~~*Phys. Chem. Chem. Phys.* ~~**17**~~**17** (46), 2015, 31247–31252.

[35] B. Nikolski and T. Tolmacheva, Permeability of membranes. II. Effect of boric anhydride and aluminium oxide on the electrode properties of glass, *Zh. Fiz. Khim* ~~**10**~~**10**, 1937, 504–512.

[36] M. Spijkman, et al., Beyond the Nernst-limit with dual-gate ZnO ion-sensitive field-effect transistors, ~~*Applied Physics Letters*~~*Appl. Phys. Lett.* ~~**98**~~**98** (4), 2011, 043502.

[37] S.H. Kim, et al., ~~Electrolyte Gated Transistors~~Electrolyte-gated transistors for ~~Organic~~organic and ~~Printed Electronics~~printed electronics, ~~*Advanced materials*~~*Adv. Mater.* ~~**25**~~**25** (13), 2013, 1822–1846.

[38] J. Rivnay, et al., Organic electrochemical transistors, ~~*Nature Reviews Materials*~~*Nat. Rev. Mater.* ~~**3**~~**3**, 2018, 17086.

Queries and Answers

Query:

Please confirm that given names and surnames have been identified correctly and are presented in the desired order, and please carefully verify the spelling of all authors.

Answer: Yes, it is ok, but the corresponding author should be my E-mail address .

Query:

Your article is registered as a regular item and is being processed for inclusion in a regular issue of the journal. If this is NOT correct and your article belongs to a Special Issue/Collection please contact k.selvaraj@elsevier.com immediately prior to returning your corrections.

Answer: Yes , it is regular issue.

Query:

Please check and confirm if the address for the corresponding author that has been added here is correct.

Answer: Now, I have corrected to reflect the right address.

Query:

Provide the closing parenthesis in the text.

Answer: OK , I have made change it .

Query:

Provide the closing parenthesis in the text.

Answer: OK , I have made change it.

Query:

Please type the full funder name and country, plus grant IDs in the text, if available. Correctly acknowledging the primary funders and grant IDs of your research is important to ensure compliance with funder policies. Have we correctly interpreted the following funding source(s) you cited in your article: “Cultural Attaché of Saudi Arabia”, “Saudi Arabia”; “Saudi Arabia”, “Saudi Arabia”?

Answer: Yes , you have replaced correctly.